Applied Physics Letters

RESEARCH ARTICLE | DECEMBER 18 2023

Ultrathin film optical coatings for all-optical mathematical operations with ultrahigh numerical aperture

Ran Wei ; Jihua Zhang ; Sohail A Jalil ; Mohamed Elkkabash ; Chunlei Guo

Appl. Phys. Lett. 123, 251102 (2023)
https://doi.org/10.1063/5.0176144

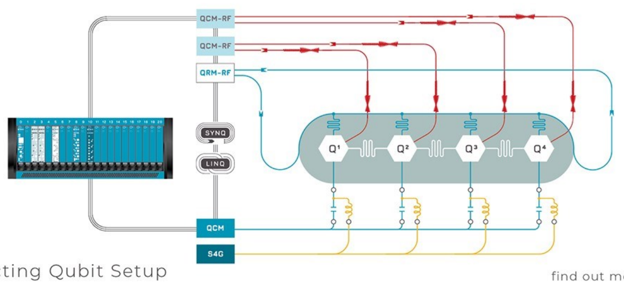

Ultrathin film optical coatings for all-optical mathematical operations with ultrahigh numerical aperture

Cite as: Appl. Phys. Lett.123, 251102 (2023); doi: 10.1063/5.0176144
Submitted: 11 September 2023 · Accepted: 28 November 2023 ·
Published Online: 18 December 2023

View Online Export Citation CrossMark

Ran Wei, Jihua Zhang,[a),b)] Sohail A Jalil,[c)] Mohamed Elkkabash,[d)] and Chunlei Guo[a)]

AFFILIATIONS

The Institute of Optics, University of Rochester, Rochester, New York 14627, USA

[a)]Authors to whom correspondence should be addressed: jhzhanghust@gmail.com and chunlei.guo@rochester.edu
[b)]Present address: ARC Centre of Excellence for Transformative Meta-Optical Systems (TMOS), Research School of Physics, The Australian National University, Canberra, ACT 2601, Australia.
[c)]Present address: Joint Attosecond Science Laboratory, National Research Council of Canada and University of Ottawa, Ottawa, Ontario K1N 6N5, Canada.
[d)]Present address: Wyant College of Optical Sciences, University of Arizona, Tucson, Arizona 85721, USA.

ABSTRACT

Optical analog computation is garnering increasing attention due to its innate parallel processing capabilities, swift computational speeds, and minimal energy requirements. However, traditional optical components employed for such computations are usually bulky. Recently, there has been a substantial shift toward utilizing nanophotonic structures to downsize these bulky optical elements. Nevertheless, these nanophotonic structures are typically realized in planar subwavelength nanostructures, demanding intricate fabrication processes and presenting limitations in their numerical apertures. In this study, we present a three-layer thin-film optical coating different from the conventional Fabry–Perot nanocavity. Our design functions as a real-time Laplacian operator for spatial differentiation, and it remarkably boasts an ultrahigh numerical aperture of up to 0.7, enabling the detected edges to be sharper and have closely matched intensities. We also experimentally demonstrate its capacity for effective edge detection. This ultracompact and facile-to-fabricate thin-film spatial differentiator holds promising prospects for applications in ultrafast optical processing and biomedical imaging. Published under an exclusive license by AIP Publishing. https://doi.org/10.1063/5.0176144

All-optical computation refers to numerical calculations of onedimensional or multidimensional information carried by optical waves.[1] Because optical waves can travel at the speed of light with virtually no interaction, optical computation can realize ultrafast and parallel calculation processes. Generally, optical computation can be categorized into two categories: digital optical computation and analog optical computation. Digital optical computation mimics the function of electronic computers, where photons promise a much larger bandwidth over electrons used in conventional computers.[2] Optical equivalents of electronic components in electronic computers were able to realize key functionalities such as logic-level restoration, cascadability, fan-out, and input–output isolation.[3] Unfortunately, the lack of energy-efficient nonlinear elements working as optical switches represents a significant hurdle for the development of efficient digital optical computing.[4] On the other hand, optical analog computation relies on linear optical processes only. This has led to a series of rapid developments in recent years, especially following the realization of a range of versatile optical technologies, such as metasurfaces,[5–7] diffractive optical elements (DOEs),[8,9] and spatial light modulators (SLMs).[10–13] In addition, optical analog computation enjoys lower or even zero power consumption. For example, it requires no power consumption for an optical lens to perform a Fourier transform between its front and back focal planes.[14] Other complex mathematical operations achieved through analog optical computation include singleorder and higher-order spatial differentiation,[15–17] integration,[18] and high/low pass filtering.[19,20] These demonstrations can find applications in optical signal processing and imaging processing.

Despite significant advancements, optical elements used for optical analog computation are bulky, which have severely limited their applications in realizing compact integrated systems.[21] The rise in nanophotonics over the past two decades, including photonic crystals,[22] high efficiency metasurfaces,[23–25] and tunable nonlocal metasurfaces,[26–28] led to the development of ultrathin and ultracompact optical analog computation devices. However, these nanophotonic devices rely on planar subwavelength nanostructures, which require intense nanofabrication that is time consuming, expensive, complex, and has low fault tolerance. Conversely, an alternative category of longitudinal nanophotonic structures based on lithography-free ultrathin film optical coatings (UFOCs) has gained prominence. This platform has matured considerably and stands as a cost-effective, scalable option in the realm of nanophotonics.[29,30] A multitude of optical functionalities have been realized using UFOCs, spanning over solar cell[31] and biosensing[32,33] developed by others and perfect light absorber,[34] gas sensing,[35] and Fano resonance[36,37] developed by us. Importantly, UFOCs have also been implemented to realize precise analog optical image processing,[38,39] further underscoring their versatility in advancing the field of nanophotonics.

Although optical spatial differentiations have been demonstrated either in the form of planar metasurfaces or longitudinal UFOCs in both 1D[40] and 2D,[41] previously reported designs have typically exhibited relatively low numerical apertures (NAs). The NA of a device plays a pivotal role in defining the device's capability to process the range of spatial frequencies from the target object collected by the imaging system according to the ideal function. Having a photonic Laplacian operator with a high NA is crucial for obtaining sharp edge information with a doublepeak pair with similar intensity. The highest NA value ever reported experimentally is 0.35.[25] Here, we propose and demonstrate a simple three-layer UFOC structure with an ultrathin absorptive layer, a lossless layer, and a metal reflector that is capable of functioning as a Laplacian operator to perform as a spatial frequency filter in 2D, with an experimentally measured NA of up to 0.7. The total thickness of the thin film

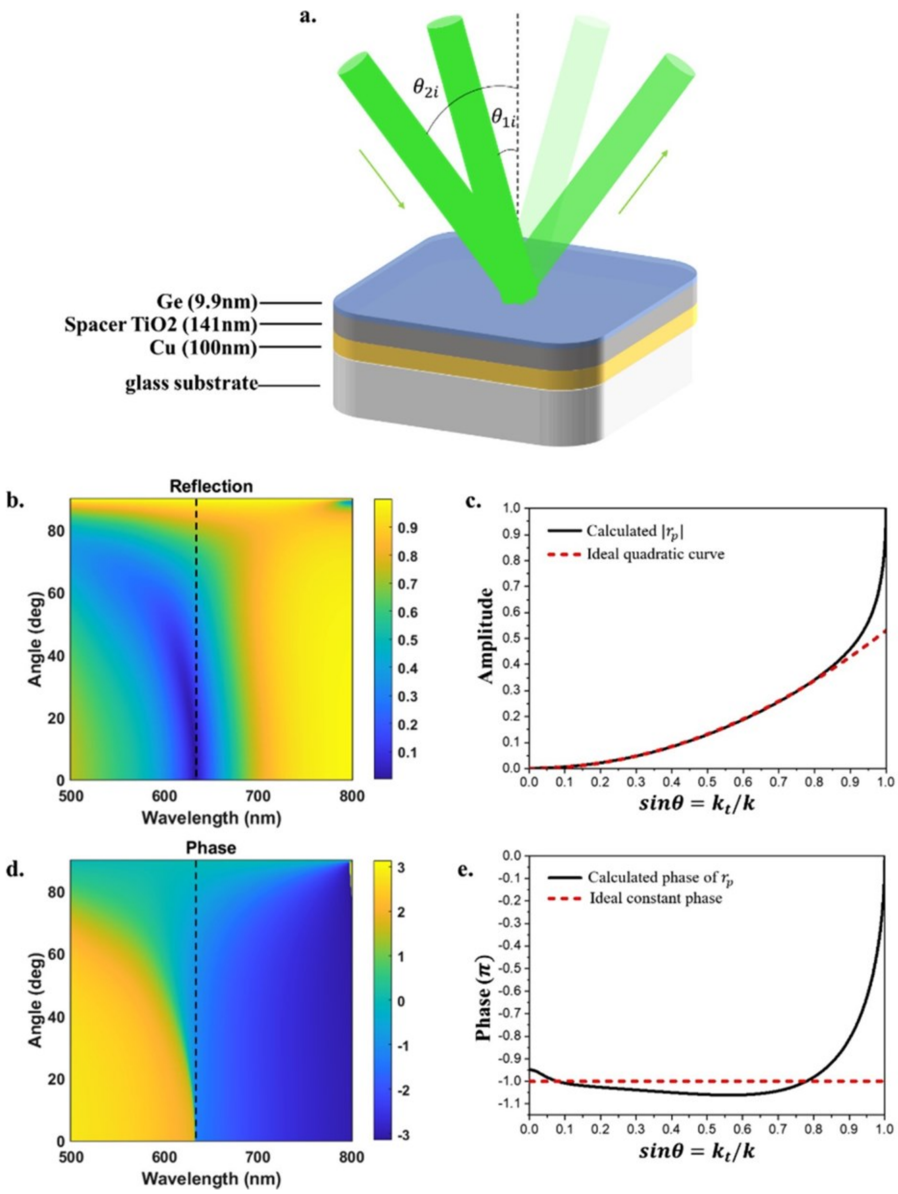

FIG. 1. Design of thin film optical coating functioning as a Laplacian operator. (a) Schematic of the proposed optical coating. Light with large incident angle (e.g., h_{2i}) is highly reflected, while light with small incident angle (e.g., h_{1i}) is absorbed. The green arrows show the propagation direction of the beam. A quadratic dependence of reflection coefficient on the incident angle performs a Laplacian operation. Calculated angular reflection (b) and phase (d) of the UFOC structure shown in (a). The UFOC structure is designed to have zero reflection at 632.8 nm for normal incidence, as indicated by the black dotted line. (c) and (e) The calculated (solid line) and ideal (dashed line) (c) reflection coefficient and phase (e) for ppolarized incident light as a function of the transverse spatial frequency (in the unit of k_0) at the design wavelength k¼ 632.8 nm. The calculated and ideal reflection coefficient are nearly identical up to a numerical aperture of 0.8, while the phase of the calculated reflection in (e) remains almost a constant in the interested spatial frequency range.

layers is 250.9nm (operating at k¼ 632.8nm). Based on the UFOC Laplacian operator, we experimentally demonstrate the edge enhancement ability of the device using an USAF-1951 resolution target. The ultra-thin thickness, high NA, and ease-of-fabrication make our proposed device as an ideal compact image processing component, e.g., to be used in portable sensing systems.[42]

In computational image processing, the Laplacian operator is often used to detect the edge of images, i.e., the high spatial frequency information carried by the images. To understand the function of the Laplacian operator, let us assume a continuous electric field propagating along the z direction in the form of

$$E = E(x, y)\exp(ik_z z); \quad (1)$$

where the amplitude of the field can be rewritten in terms of the spatial frequencies as an inverse Fourier transform,

$$E = \iint_{-\infty}^{+\infty} \tilde{E}(k_x, k_y)\exp(ik_x x + ik_y y)\,dk_x\,dk_y\,\exp(ik_z z). \quad (2)$$

If we then apply the transverse 2D Laplacian operator to the field, we have

$$\nabla^2 E = \frac{\partial^2 E}{\partial x^2} + \frac{\partial^2 E}{\partial y^2} = \iint_{-\infty}^{+\infty} -k_t^2\,\tilde{E}(k_x, k_y)\exp(ik_x x + ik_y y)\,dk_x\,dk_y\,\exp(ik_z z). \quad (3)$$

Here, $k_t = \sqrt{k_x^2 + k_y^2} = k\sin\theta$ represents the transverse spatial frequency of an incident plane wave with wave number k and an incident angle θ, and $\tilde{E}(k_x, k_y)$ is the spatial Fourier transform of input field $E(x, y)$. Our goal is to create a mirror that performs a Laplacian operation on the reflected field. Accordingly, the amplitude of the reflection coefficient of this mirror must have a quadratic dependence with respect to the transverse spatial frequency, i.e., $r \propto k^2\sin^2\theta$. Ideally, the phase response should be constant. In practice, a quasi-constant phase term could also be extracted out of the integral, leaving no influence on the final result.[14] This means that the low spatial frequency information, i.e., the background information of the images propagating with a small k_t, will have low reflectance. However, high spatial frequency information, i.e., the edge information of an image propagating at a large k_t; will have high reflectance. Applying a Laplacian operator on an image, thus, can also perform edge detection.

In this paper, the Laplacian operator was designed based on a stack of thin film optical coatings consisting of 9.9nm germanium (Ge) as the absorptive layer, 141 nm titanium dioxide (TiO_2) as the lossless layer, and 100 nm copper (Cu) as the metal reflector on top of a glass substrate, as shown in Fig. 1(a). The proposed optical coating supports a resonance, i.e., a reflection dip, at normal incidence at a wavelength of $\lambda = 632.8$nm due to multi-beam destructive interference at the air-Ge interface and optical absorption in the Ge layer. TiO_2 serves as a spacer layer to provide the phase difference necessary for total destructive interference, so that perfect light absorption is realized for normal incidence at the desired resonance wavelength (see detailed calculations in the supplementary material). The bottom Cu layer is designed to be thick enough so that there will be no transmitted light. Different from the Fabry–Perot nanocavity employing the cavity mode to support the resonant spectral response, our design stems from a simple optical coating that does not rely on cavity mode with a pronounced absorption peak, where a highly absorptive dielectric is deposited atop a metal reflector (see Fig. S3 for more details).[43] Nevertheless, perfect absorption is hard to achieve due to the inadequate phase difference at the interface. The presence of the lossless spacer layer is thus crucial to compensate for the phase mismatch for realizing total destructive interference.[44] Since the reflection coefficients at the TiO_2-Cu and Ge-TiO_2 interfaces and the propagation

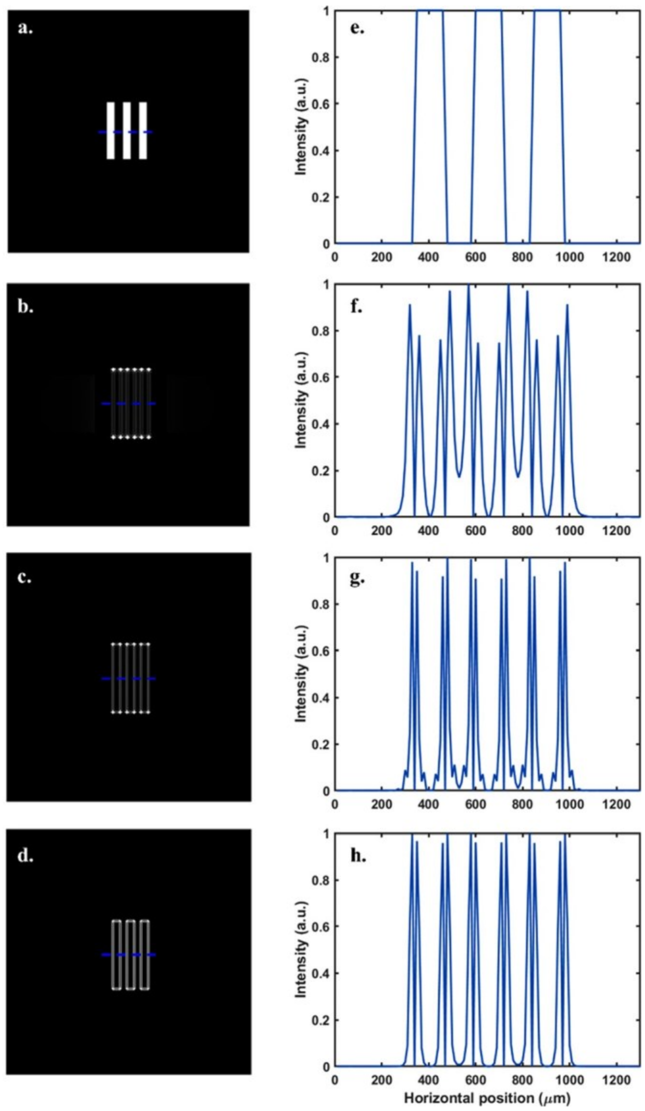

FIG. 2. Numerical calculations for edge detection under different NA of the UFOC for an object with the width of 200 Ɩm for each stripe. (a)–(d) Original object and simulated edge detection results for UFOC with NA of 0.1, 0.3, and 0.8, respectively. The NA of the imaging system is kept at 1 for all calculations. (e) –(h) Cross sections of the original object and edge detection in (a) –(d) indicated by the blue dotted line, where the two peaks corresponding to each individual edge are sharper and have more closely matched intensities as the NA of UFOC increases.

phase accumulation inside the TiO_2 layer are angle dependent, so is the resonance wavelength and the reflection at a certain wavelength [Fig. 1(b)]. Figures 1(c) and 1(e) show the amplitude and phase of the reflection coefficient calculated from the surface of the designed thin film structures for the p-polarized light as a function of the angle of incidence at the resonant wavelength k ¼ 632:8 nm, respectively. The reflection coefficient shows an excellent fit to a quadratic curve up to 53 deg, which corresponds to a numerical aperture of NA¼ 0.8 for the UFOC, while the phase of the reflected beam remains almost constant in the interested region. Consequently, the thin film structure performs Laplacian operation on the incident field. For s-polarized light, the reflection coefficient also enjoys a quadratic relation up to an NA ¼ 0.5 (see the supplementary material).

To highlight the importance of the demonstrated high NA of the UFOC device, we numerically calculated the edge detection performance of a photonic Laplacian operator on an object in Fig. 2(a) with NA of 0.1, 0.3, and 0.8, as shown in Figs. 2(b)–2(d), respectively. Importantly, the NA of the imaging system was maintained at a constant value (NA¼ 1) across all calculations. Due to the nature of the second derivatives, there will be two peaks corresponding to each edge.[45] We further scrutinized the edge-detection outcomes by plotting cross sections in Figs. 2(f)–2(h). This analysis effectively illustrates that as the NA of the photonic Laplacian operator increases, the two peaks associated with each edge in the object exhibit narrower linewidths and more closely matched intensities. This trend aligns with the pursuit of a more ideal edge-detection outcome, highlighting the crucial role played by the elevated NA of the photonic Laplacian operator in our UFOC device (see Fig. S4 for more discussion).

The proposed UFOC device is fabricated by sequentially depositing Cu (100nm), TiO_2 spacer layer (141nm), and a thin layer of Ge (9.9nm) on a glass substrate by e-beam evaporation using Kurt Lesker's KLJ PVD75 (hybrid) system. Under the pressure of 5 10^6Torr, deposition rates of 1, 0.8, and 0.1A_ /s were used for the Cu, TiO_2, and Ge layers, respectively. The refractive index of TiO_2 and Ge obtained from ellipsometry using V-VASE ellipsometer (J. A. Woollam) is shown in supplementary material and used for UFOC design. The reflectance spectrum under ppolarization was measured using the same ellipsometer as shown in Fig. 3(a). Due to limitations of the spectrometer, the angle of incidence can only be measured between 15 and 75. From Fig. 3(b), we can see the absorption at 605nm is 96% for 15, which closely agrees with the simulated angular reflection [Fig. 1(b)]. The difference between the experimental and simulated results is due to differences in the as-deposited refractive index, thickness, and film uniformity. A more detailed discussion can be found in supplementary material. The reflectance at the resonant wavelength for different incident angles is fitted by a quartic curve (reflectance is proportional to j jr$_p$ ^{2}) up to an NA of 0.7, as shown in Fig. 3(b).

To experimentally verify the Laplacian operator capability of our UFOC device, we demonstrate the edge enhancement using a negative USAF-1951 resolution target (Thorlabs R1DS1N). The experimental setup for testing the sample is shown in Fig. 4.

Broadband illumination was adopted using a sapphire crystal that generates supercontinuum white light from a Ti:sapphire femtosecond laser centered at 800 nm. The preferred spectral range was then selected by a bandpass filter centered at 605 nm, followed by a Glan–Thompson polarizer (Melles Griot: 03 PTH 112/C and wavelength range: 350–2300 nm) to obtain p-polarized illumination. In order to fit the beam to the object, the beam was reshaped three times smaller through a two-lens telescope and then illuminated onto the group 1 and element 2line patterns with 220 lm width for each line. To project the object onto the thin-film structure, we employed the benchtop K€ohler-illumination configuration, where the collimated beam through the object is transmitted through a telescope consisting of a f¼ 100 mm lens, a beam splitter, and a NA ¼ 0.8 Nikon 60 microscope objective. This telescope enabled a 40 demagnification of the image, allowing more spatial frequencies to be collected by the UFOC under test. The beam splitter serves to direct the reflected image into the couple-charged device (CCD, ZWO ASI178MM) for the final imaging. To be noticed, the higher-order diffractions from the resolution target, whose polarization would be altered as a mixture of p- and s-polarized light,[46] were not collected by the projecting system, and therefore, the polarization of the beam was unchanged within the setup.

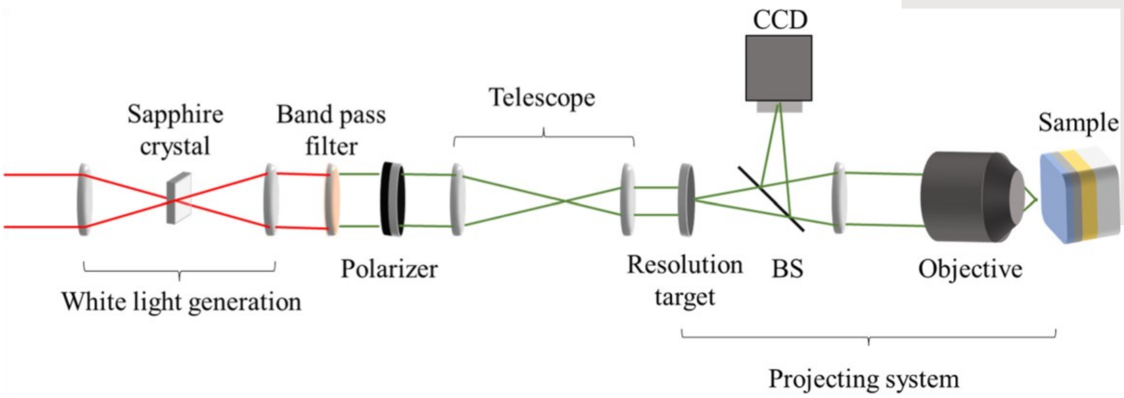

FIG. 4. Experimental setup for testing the sample's edge enhancement function. In order to have the desired wavelength, we shined a fs-laser onto a sapphire crystal to generate supercontinuum white light. A bandpass filter centered at 605 nm was then used to filter out the target wavelength. The beam was projected onto a negative 1951 USAF test target after being compressed by a two-lens telescope. Finally, the test target was projected onto the sample through a projecting system. The differentiated image was then collected by the charged coupled device (CCD).

To demonstrate the edge enhancement of the sample, the resolution target was placed at the front focal plane of the f¼ 100mm lens, and the results clearly indicated edge enhancement of the pattern of interest at the resonance wavelength k¼ 605 nm [Fig. 5(b)]. The experimental observations are consistent with the numerical results mentioned in the previous sections.

To further confirm the Laplacian operation capability of the designed structure, we compared the intensity from the same part of the two images in Figs. 5(a) and 5(b). The image intensity on the cutting line is presented in Fig. 5(c), where the blue and yellow curves indicate the normal imaging when putting a metallic mirror at the position of sample and imaging obtained from the UFOC structure, respectively. The orange curve is the ideal second derivative of the object, which is calculated from the blue curve. Due to the nature of the second derivatives, we observed two peaks corresponding to each edge of the object.[45] By comparing the three curves, we can see that the UFOC structure has achieved the function of a Laplacian operator, showing a clear 2-peak pattern for each edge. The difference between the experimental results and the ideal second derivative comes from the effects of non-monochromatic and non-uniform illumination onto the UFOC. These effects are discussed in detail in the supplementary material. Despite the non-ideal illumination source, the key feature of the Laplacian operation is reserved in our designed UFOC.

In summary, we have conducted comprehensive numerical and experimental investigations, presenting a large-scale, lithography-free, and cost effective UFOC device designed for real-time all-optical Laplacian operations that is different from conventional metal–dielectric–metal configuration. Our study encompassed a detailed characterization of the angular-dependent response of the UFOC

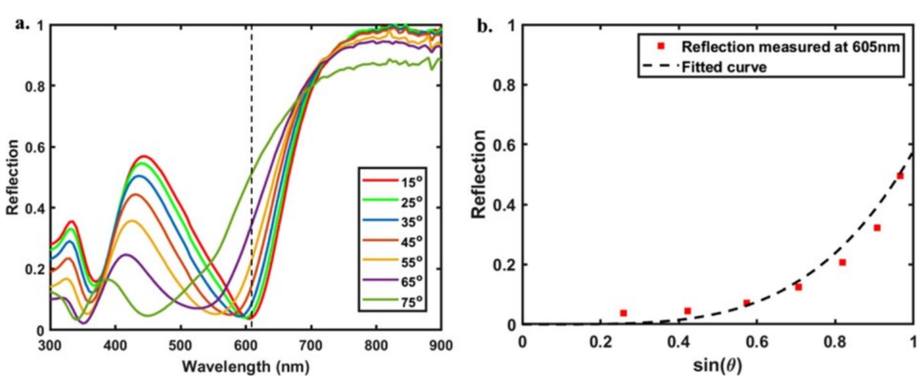

FIG. 3. Response of the angle-dependent reflection of the fabricated sample, where both the broadband response (a) and the response at the resonant wavelength (b) are presented. The dotted line in (a) represents the response at the resonant wavelength. The asterisk in (b) implies the actual measurement by spectrometer at 605 nm, while the black dotted line represents the fitting curve based on the measurement. The reflection response of the sample perfectly fits a quartic curve of 0:58sin^{4}h for the numerical aperture as large as 0.7.

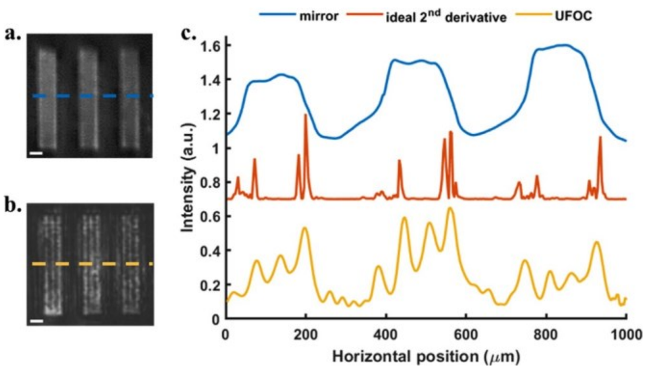

FIG. 5. Verification on the Laplacian operator function of the sample. (a) Image of the resolution target obtained through a metallic mirror put at the sample position. (b) Image of the same part of the resolution target under the illumination centered at the resonant wavelength k ¼ 605 nm, where only the edge of the object is displayed. The scale bars in (a) and (b) are 200 lm. (c) Comparison of the experimental and calculated second order differentiated intensity from the two images, denoted by the blue line (imaging from metallic mirror), the orange line (ideal second-order differentiated intensity), and yellow line (imaging from the sample), respectively.

when operating in the reflection mode, accompanied by an evaluation of its capability for edge detection as a Laplacian operator. We have experimentally demonstrated effective edge detection and secondorder differentiation, using a USAF 1951 resolution target. More importantly, we have experimentally realized an ultrahigh numerical aperture of up to 0.7. This UFOC device provides a more accurate second-order derivative edge detection.

See the supplementary material that provides the material property and detailed analysis on the experimental results.

AUTHOR DECLARATIONS Conflict of Interest

The authors have no conflicts to disclose.

Author Contributions

Ran Wei: Formal analysis (equal); Investigation (equal); Writing – original draft (equal); Writing – review & editing (equal). Jihua Zhang: Conceptualization (equal); Writing – review & editing (equal). Sohail A. Jalil: Investigation (supporting). Mohamed Elkkabash: Investigation (supporting); Writing – review & editing (equal).
Chunlei Guo: Funding acquisition (lead); Supervision (lead).

DATA AVAILABILITY

The data that support the findings of this study are available from the corresponding authors upon reasonable request.

REFERENCES

[1]S. Abdollahramezani, O. Hemmatyar, and A. Adibi, "Meta-optics for spatial optical analog computing," Nanophotonics 9, 4075–4095 (2020). [2]D. R. Solli and B. Jalali, "Analog optical computing," Nat. Photonics 9, 704–706 (2015). [3] A. Miller, K. Welford, and B. Daino, Nonlinear Optical Materials and Devices for Applications in Information Technology (Springer Science & Business Media, 2013), Vol. 289.
[4]R. S. Tucker, "The role of optics in computing," Nat. Photonics 4, 405–405 (2010).
[5]G. Zheng, H. Muhlenbernd, M. Kenney€ et al., "Metasurface holograms reaching 80% efficiency," Nat. Nanotechnol. 10, 308–312 (2015).
[6]X. Ni, A. V. Kildishev, and V. M. Shalaev, "Metasurface holograms for visible light," Nat. Commun. 4, 1–6 (2013).
[7]J. Zhang, M. Elkabbash, R. Wei et al., "Plasmonic metasurfaces with 42.3% transmission efficiency in the visible," Light. Sci. Appl. 8, 53 (2019).
[8]A. Goncharsky, A. Goncharsky, and S. Durlevich, "Diffractive optical element for creating visual 3D images," Opt. Express 24, 9140–9148 (2016).
[9]L. Wang, T. Tschudi, T. Halldorsson, and P. R. Petursson, "Speckle reduction in laser projection systems by diffractive optical elements," Appl. Opt. 37, 1770–1775 (1998).
[10]S. Iwasa, "Optical processing: A near real-time coherent system using two Itek PROM devices," Appl. Opt. 15, 1418–1424 (1976).
[11]D. S. Oliver, "Real-time spatial modulators for optical/digital processing systems," Opt. Eng. 17, 173288 (1978).
[12]W. Bleha, L. Lipton, E. Wiener-Avnear et al., "Application of the liquid crystal light valve to real-time optical data processing," Opt. Eng. 17, 174371 (1978).
[13]G. Labrunie, J. Robert, and J. Borel, "A 128 128 electro-optical interface for real time data processing," Rev. Phys. Appl. 10, 143–146 (1975).
[14] J. W. Goodman, Introduction to Fourier Optics, 3rd ed. (Roberts and Company Publishers, 2005).
[15]N. V. Golovastikov, D. A. Bykov, and L. L. Doskolovich, "Resonant diffraction gratings for spatial differentiation of optical beams," Quantum Electron. 44, 984 (2014).
[16]T. Zhu, Y. Lou, Y. Zhou et al., "Generalized spatial differentiation from the spin hall effect of light and its application in image processing of edge detection," Phys. Rev. Appl. 11, 034043 (2019).
[17]D. Xu, S. He, J. Zhou et al., "Optical analog computing of two-dimensional spatial differentiation based on the Brewster effect," Opt. Lett. 45, 6867–6870 (2020).
[18]E. A. Bezus, L. L. Doskolovich, D. A. Bykov, and V. A. Soifer, "Spatial integration and differentiation of optical beams in a slab waveguide by a dielectric ridge supporting high-Q resonances," Opt. Express 26, 25156–25165 (2018).
[19]J. H. Zhu, Q. J. Wang, P. Shum, and X. G. Huang, "A nanoplasmonic high-pass wavelength filter based on a metal-insulator-metal circuitous waveguide," IEEE Trans. Nanotechnol. 10, 1357–1361 (2011).
[20] D. Correas-Serrano, J. S. Gomez-Diaz, J. Perruisseau-Carrier, and A. AlvarezMelcon, "Graphene-based plasmonic tunable low-pass filters in the terahertz band," IEEE Trans. Nanotechnol. 13, 1145–1153 (2014).
[21]F. Zernike, "Phase contrast, a new method for the microscopic observation of transparent objects," Physica 9, 686–698 (1942).
[22]J. D. Joannopoulos, P. R. Villeneuve, and S. Fan, "Photonic crystals: Putting a new twist on light," Nature 386, 143–149 (1997).
[23]Y. Zhou, H. Zheng, I. I. Kravchenko, and J. Valentine, "Flat optics for image differentiation," Nat. Photonics 14, 316–323 (2020).
[24]J. Zhou, H. Qian, C.-F. Chen et al., "Optical edge detection based on highefficiency dielectric metasurface," Proc. Natl. Acad. Sci. U. S. A. 116, 11137–11140 (2019).
[25]A. Cordaro, H. Kwon, D. Sounas et al., "High-index dielectric metasurfaces performing mathematical operations," Nano Lett. 19, 8418–8423 (2019).
[26]T. Xiao, H. Yang, Q. Yang et al., "Realization of tunable edge-enhanced images based on computing metasurfaces," Opt. Lett. 47, 925–928 (2022).

[27]S. C. Malek, A. C. Overvig, S. Shrestha, and N. Yu, "Active nonlocal metasurfaces," Nanophotonics 10, 655–665 (2020).
[28]I. Khodasevych, L. Wesemann, A. Roberts, and F. Iacopi, "Tunable nonlocal metasurfaces based on graphene for analogue optical computation," Opt. Mater. Express 13, 1475–1487 (2023).
29 K. Sreekanth, M. ElKabbash, V. Caligiuri et al., New Directions in Thin Film Nanophotonics (Springer, 2019), Vol. 1.
30 H. A. Macleod and H. A. Macleod, Thin-Film Optical Filters (CRC Press, 2010).
[31]M. A. Green, "Thin-film solar cells: Review of materials, technologies and commercial status," J. Mater. Sci. 18, 15–19 (2007).
[32]K. V. Sreekanth, S. Sreejith, S. Han et al., "Biosensing with the singular phase of an ultrathin metal-dielectric nanophotonic cavity," Nat. Commun. 9, 1–8 (2018).
[33]V. Tvarozek, T. Hianik, I. Novotny et al., "Thin films in biosensors," Vacuum 50, 251–262 (1998).
[34]J. Zhang, R. Wei, M. Elkabbash et al., "Thin-film perfect infrared absorbers over single- and dual-band atmospheric windows," Opt. Lett. 45, 2800 (2020).
[35]M. ElKabbash, K. V. Sreekanth, A. Fraiwan et al., "Ultrathin-film optical coating for angle-independent remote hydrogen sensing," Meas. Sci. Technol. 31, 115201 (2020).
[36]M. ElKabbash, T. Letsou, S. A. Jalil et al., "Fano-resonant ultrathin film optical coatings," Nat. Nanotechnol. 16, 440–446 (2021).
[37]M. Elkabbash, N. Hoffman, A. R. Lininger et al., "Fano resonant optical coatings platform for full gamut and high purity structural colors," Nat. Commun. 14, 3960 (2023).
[38]Y. Zhou, J. Zhan, R. Chen et al., "Analogue optical spatiotemporal differentiator," Adv. Opt. Mater. 9, 2002088 (2021).
[39]W. Wu, W. Jiang, J. Yang et al., "Multilayered analog optical differentiating device: Performance analysis on structural parameters," Opt. Lett. 42, 5270–5273 (2017).
[40]T. Zhu, Y. Zhou, Y. Lou et al., "Plasmonic computing of spatial differentiation," Nat. Commun. 8, 1–6 (2017).
[41]L. Wesemann, E. Panchenko, K. Singh et al., "Selective near-perfect absorbing mirror as a spatial frequency filter for optical image processing," APL Photonics 4, 100801 (2019).
[42]D. N. Breslauer, R. N. Maamari, N. A. Switz et al., "Mobile phone based clinical microscopy for global health applications," PloS One 4, e6320 (2009).
[43]M. A. Kats, R. Blanchard, P. Genevet, and F. Capasso, "Nanometre optical coatings based on strong interference effects in highly absorbing media," Nat. Mater. 12, 20–24 (2013).
[44]H. Song, L. Guo, Z. Liu et al., "Nanocavity enhancement for ultra-thin film optical absorber," Adv. Mater. 26, 2737–2743 (2014).
45 A. C. Bovik, Handbook of Image and Video Processing (Academic Press, 2010).
[46]M. Mansuripur, "Distribution of light at and near the focus of high-numericalaperture objectives," J. Opt. Soc. Am. A 3, 2086–2093 (1986).